$Two-step\ chemical\ looping\ cycle\ for\ renewable\ NH_3\ production\ based\ on\ non-catalytic\ Co_3Mo_3N/Co_6Mo_6N\ reactions$

Nhu Pailes Nguyen¹, Shaspreet Kaur¹, H. Evan Bush², James E. Miller³, Andrea Ambrosini², Peter G. Loutzenhiser^{1*}

¹George W. Woodruff School of Mechanical Engineering, Georgia Institute of Technology, Atlanta, Georgia USA, 30332-0405

²Concentrating Solar Technologies, Sandia National Laboratories, P.O. Box 5800, Albuquerque, NM 87185-1127 USA

³ASU LightWorks, Arizona State University, PO Box 875402, Tempe, AZ 85287-5402, USA *Corresponding Author: Peter G. Loutzenhiser, Email: peter.loutzenhiser@me.gatech.edu Phone: +1.404.894.3012

Summary

A two-step solar thermochemical looping cycle based on Co₃Mo₃N/Co₆Mo₆N reduction/nitridation reactions offers a pathway for green NH₃ production that utilizes concentrated solar irradiation, H₂O, and air as feedstocks. The NH₃ production cycle steps both derive process heat from concentrated solar irradiation and encompass (1) the reduction of Co₃Mo₃N in H₂ to Co₆Mo₆N and NH₃; and (2) nitridation of Co₆Mo₆N to Co₃Mo₃N with N₂. Co₃Mo₃N reduction/nitridation reactions were examined at different H₂ and/or N₂ partial pressures and temperatures. NH₃ production was quantified in-situ using liquid conductivity measurements coupled with mass spectrometry. Solid state characterization was performed to identify a surface oxygen layer that necessitated the addition of H₂ during cycling to prevent surface oxidation by trace amounts of O₂. H₂ concentrations of > 5% H₂/Ar and temperatures >500 °C were required to reduce Co₃Mo₅N to Co₆Mo₆N and form NH₃ at 1 bar. Complete regeneration of Co₃Mo₃N from Co₆Mo₆N was achieved at conditions of 700 °C under 25 to 75% H₂/N₂. H₂ pressure-swings were observed to increase NH₃ production during Co₃Mo₃N reduction. The results represent the first comprehensive characterization of and definitive non-catalytic production of NH₃ via chemical looping with metal nitrides and provide insights for technology development.

Keywords: Co₃Mo₃N, Co₆Mo₆N, NH₃ synthesis, concentrating solar technologies, chemical looping.

1. Introduction

NH₃ is a vital component for agricultural fertilizer and is an energy dense, carbon-free chemical and potential fuel [1]. NH₃ is currently produced with the Haber-Bosch process, which is highly energy intensive and accounts for ~2% of global energy consumption and 1.3% of global CO₂ emission [2]. NH₃ production with the Haber-Bosch process with H₂ and N₂ occurs at elevated pressures >100 bar and at temperatures between 425 and 450 °C with the aid of metal catalysts (*e.g.*, fused-iron [3]). H₂ is commonly produced via CH₄ reforming with H₂O(v) [4], and N₂ is commonly derived from air via the combustion of CH₄ to oxidize O₂ to CO₂, where CO₂ is subsequently removed.

NH₃ chemical thermodynamics favor high pressures and intermediate to low temperatures to avoid decomposition to N₂ and H₂. The temperatures used are dictated by the reaction kinetics for most applications. High pressures are required to compensate for elevated temperatures with significant yields possible despite the unfavorable thermodynamics according to Le Chatelier's principle. The need to reduce the carbon footprint associated with NH₃ production combined with the required elevated temperatures and pressures make it ideally suited for integration with concentrated solar thermal (CST) technologies.

Chemical looping NH₃ production/synthesis (CLAP/CLAS) processes have been examined to reduce the energy requirements of Haber-Bosch. CLAP typically involves hydrogenating nitrogen carriers to produce NH₃, and N₂ is used to replenish lattice nitrogen, closing the chemical loop. N₂ sourced from lattice nitrogen is activated on the material surface during the hydrogenation, reducing the elevated pressure and temperature requirement compared to Haber-Bosch. Comprehensive reviews of CLAP technologies were previously performed by [5-7], where CLAP was divided into three major pathways: (1) hydrogenation of metal nitrides using H₂, (2) hydrogenation of metal nitrides using H₂O, and (3) hydrogenation of metal hydrides and imides [8] using H₂. Reducing metal nitrides using H₂ was identified as a less complex approach to produce NH₃, commonly limited to two cycle steps [6]. This pathway utilizes transition metal

nitrides (Mo_xN, M_xN_y, Co₃Mo₃N, Fe₃Mo₃N, etc.) or ionic metal nitrides (Li₃N, Ca₃N₂, Sr₂N, etc.) as nitrogen carriers.

Metal nitrides have also been previously examined as catalysts to improve NH₃ production from N₂ and H₂, where the lattice nitrogen is not consumed in the reaction, described with a Mars–Van Krevelen mechanism [9-12]. Co₃Mo₃N [13, 14] and Cs-promoted Co₃Mo₃N [14] were identified as more effective catalysts for NH₃ production compared to other ternary nitrides (*e.g.*, Ni-Mo-N or Fe-Mo-N [13]), as the Co-Mo combination resulted in an optimal nitrogen adsorption energy for NH₃ production [15]. NH₃ synthesis was observed to be significantly impacted by the Co₃Mo₃N synthesis methodology and gas pre-treatment under 75% H₂/N₂ at temperatures > 600 °C, which resulted in a more active catalyst [14, 16]. Nitrogen isotopic exchange pathways were previously investigated to elucidate reactivity of gas phase and lattice nitrogen in Co₃Mo₃N [17]. N₂ activation and exhange rates were identified as the rate limiting mechanisms in NH₃ production using Co₃Mo₃N as catalyst. The presence of H₂ has been observed to influence isotopic scrambling rates (*e.g.*, Ru, K), which accounts for the importance of H₂ presence in the metal nitride nitridation reaction in an H₂/N₂ environment where the metal nitride nitrogen incorporation rates are affected by H₂ partial pressures.

Non-catalytic behavior of Co₃Mo₃N was observed where 50% of lattice nitrogen was removed when reacted with H₂ to form a metastable reduced phase of Co₆Mo₆N [10, 13, 18-20]. Reacting Co₆Mo₆N with N₂ completely replenished the lattice nitrogen back to Co₃Mo₃N [18]. Previous work showed Co₃Mo₃N as an effective nitrogen transfer reagent [10, 20] with evidence of NH₃ production when reducing Co₃Mo₃N under 75% H₂/Ar. Co₃Mo₃N cyclability and nitrogen capacity are suitable for solar thermochemical looping to produce NH₃ from H₂ and N₂, with potential for producing more NH₃ compared with Co₃Mo₃N catalysis alone under reduced pressures.

Two-step solar thermochemical looping cycle for renewable NH₃ production

Renewable NH₃ production via a two-step solar thermochemical looping cycle based on Co₃Mo₃N/Co₆Mo₆N reactions using concentrated solar irradiation to provide process heat is an attractive alternative that enables operation at reduced pressures compared to Haber-Bosch. The first step of the cycle is the chemical reduction of Co₃Mo₃N with H₂ to produce NH₃, represented as:

$$4\text{Co}_3\text{Mo}_3\text{N} + 3\text{H}_2 \rightarrow 2\text{Co}_6\text{Mo}_6\text{N} + 2\text{NH}_3$$
 (1a)

The second step is the nitridation of Co_6Mo_6N using N_2 derived from solar thermochemical air separation, represented as:

$$2\text{Co}_6\text{Mo}_6\text{N} + \text{N}_2 \rightarrow 4\text{Co}_3\text{Mo}_3\text{N}$$
 (1b)

The Co₃Mo₃N is recycled back to the first step to complete the cycle, resulting in an overall reaction, represented as:

$$N_2 + 3H_2 \rightarrow 2NH_3 \tag{2}$$

The schematic of the complete cycle is shown in Figure 1. The thermochemical looping cycle becomes renewable when the N_2 is derived from solar thermochemical air separation [21-24], the H_2 from solar thermochemical H_2 O splitting [25-27], and the process heat from CST [28, 29].NH₃ production was previously proposed with a fixed particle bed reactor directly coupled to CST technologies [30]. Technoeconomic analysis showed the potential of the proposed plant to achieve a target price of < \$250/ton of NH₃ without including H_2 cost.

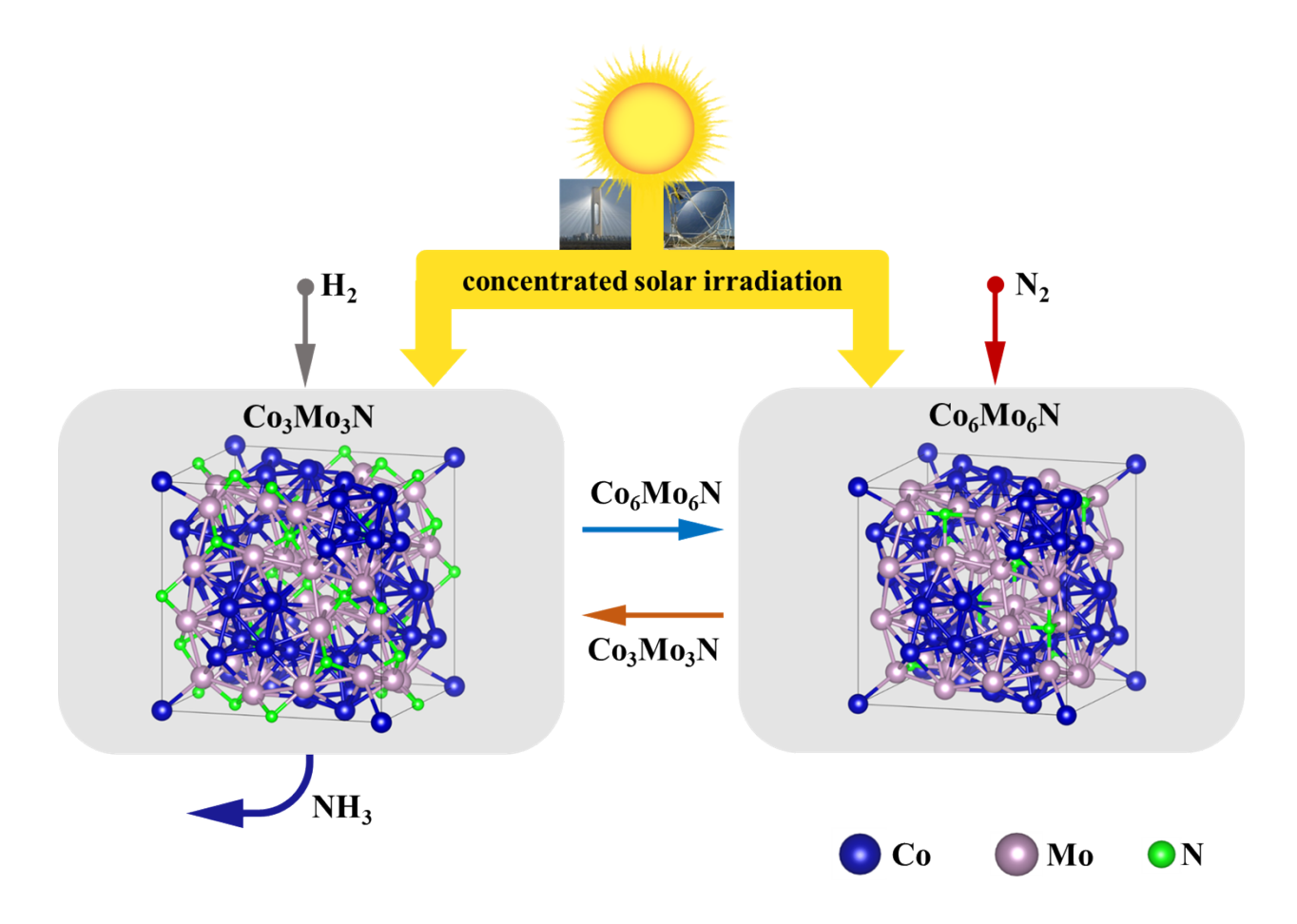


Figure 1. Schematic of Co₃Mo₃N and Co₆Mo₆N reduction/nitridation reactions for concentrating solar thermochemical NH₃ production cycle.

Limited knowledge is available pertaining to optimal conditions to maximize reaction rates and NH₃ yield via Co₃Mo₃N/Co₆Mo₆N reduction/nitridation. The focus of this work was to characterize the Co₃Mo₃N/Co₆Mo₆N reaction by examining nitrogen capacities at different temperatures and N₂ partial pressures, to quantify temporal NH₃ production, and to gain insight into reaction mechanisms and limitations for informing reactor design and operations.

Co₃Mo₃N powder samples were characterized using a combination of powder x-ray diffraction (PXRD or XRD, PANalytical X'Pert PRO Alpha-1 diffractometer with Cu Kα radiation), scanning electron microscopy coupled with energy dispersive X-ray spectroscopy (SEM/EDS, Phenom ProX G5), elemental analysis, x-ray photoelectron spectroscopy (XPS, Thermo K-Alpha, Al K-Alpha source), and transmission electron microscopy (TEM, Hitachi HD2700). Reduction/nitridation temperature and H₂ pressure-swings were performed using a tube

furnace reactor (MTI GSL-1700X) to investigate sample nitrogen capacities at varying temperatures and H_2 and/or N_2 partial pressures. NH_3 was detected and quantified using a combination of mass spectrometry (MS, OmniStar GSD 320) and liquid conductivity measurements (Orion Star A212, Thermo Fisher Scientific) where favorable conditions to minimize NH_3 dissociation were examined.

2. Results and Discussion

2.1 Material characterization

Nitride sample compositions are identified using the standard first-letter convention followed by numbers indicating their stoichiometry for simplicity: $Co_3Mo_3N \equiv CMN331$; $Co_6Mo_6N \equiv CMN661$.

Elemental analysis: Elemental analysis was performed with inductively coupled plasma - optical emission spectrometry (ICP-OES, Perkin-Elmer Optima 5300 DV) and combustion analysis (Perkin-Elmer 2400 Series II CHNS/O Analyzer) to verify elemental compositions. An unreduced and a fully reduced samples were identified as Co_{3.00}Mo_{3.10}N_{1.13} and Co_{6.00}Mo_{6.17}N_{0.95}, respectively, matching the expected stoichiometry for CMN331 and CMN661, respectively.

X-ray diffractometry: The XRD patterns are shown in Figure 2 for (a) a CMN331 powder sample reduced at 700 °C under 75% H_2 /Ar for 4 h (red line) compared against the unreduced sample (blue line) and a cubic Co_3Mo_3N reference pattern (PDF4+ 01-080-3329, black lines) and (b) a CMN331 powder sample reduced under 75% H_2 /Ar at 700 (red line) and 650 °C (green line) for 4 h compared against a cubic Co_6Mo_6N reference pattern (PDF4+ 04-017-2710, black lines). Unreduced CMN331 samples were matched to cubic Co_3Mo_3N reference pattern (PDF4+ 01-080-3329), and fully reduced samples similar to the top pattern (Fig. 2a) were matched to cubic Co_6Mo_6N (PDF4+ 04-017-2710) reference pattern. Offsets between CMN331 and CMN661 phases (Fig. 2b) were clearly observed at $2\theta < 50^\circ$ for partially reduced samples. Partially reduced samples were identified by presence of both CMN331 and CMN661 phases [18], as seen in the second pattern (Fig. 2b).

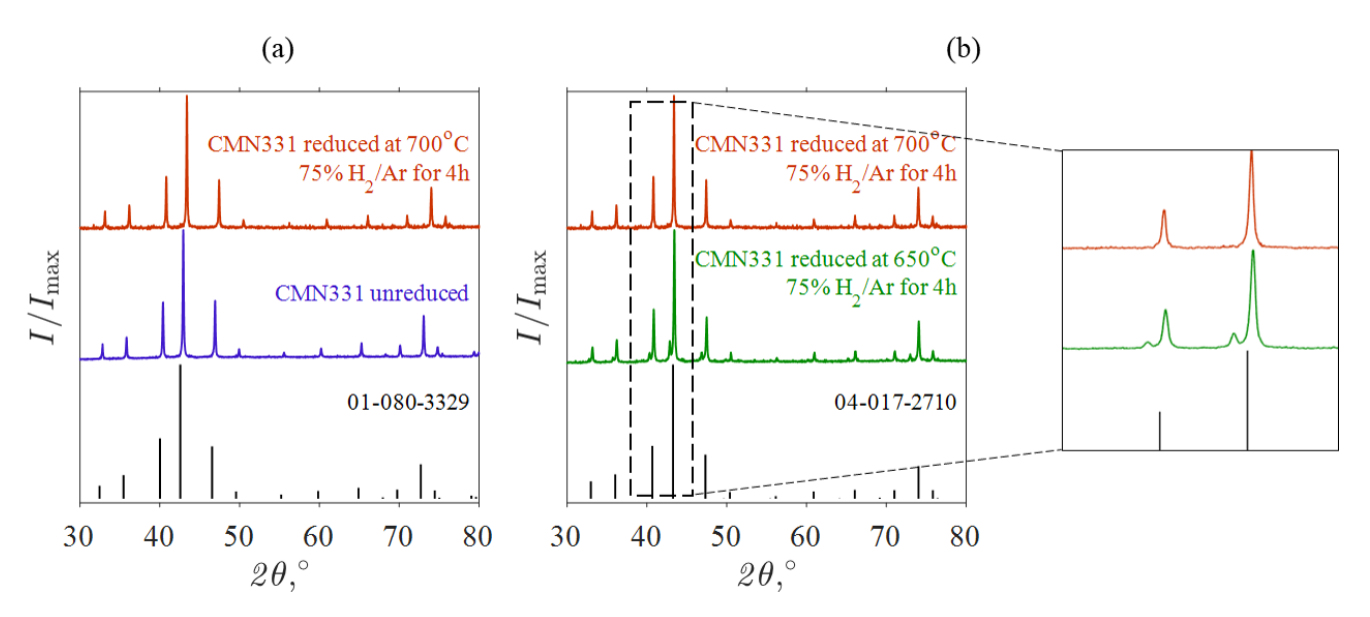


Figure 2. Normalized XRD intensity as a function of 2θ comparing (a) Co₃Mo₃N before and after H₂ pressure-swing reduction experiments at 700 °C and (b) Co₃Mo₃N after pressure-swing reduction experiments at 650 and 700 °C. Samples were compared against existing Co₃Mo₃N (PDF4+ 01-080-3329) and Co₆Mo₆N (PDF4+ 04-017-2710) reference patterns.

Elemental distribution and particle morphology: Needle-like morphologies were observed under SEM, as shown in Figure 3, for a CMN331 sample (a) before and (b) after cycling. No noticeable changes in particle morphologies were observed after the samples were subjected to thermal cycling up to 700 °C, although with some evidence of agglomeration.

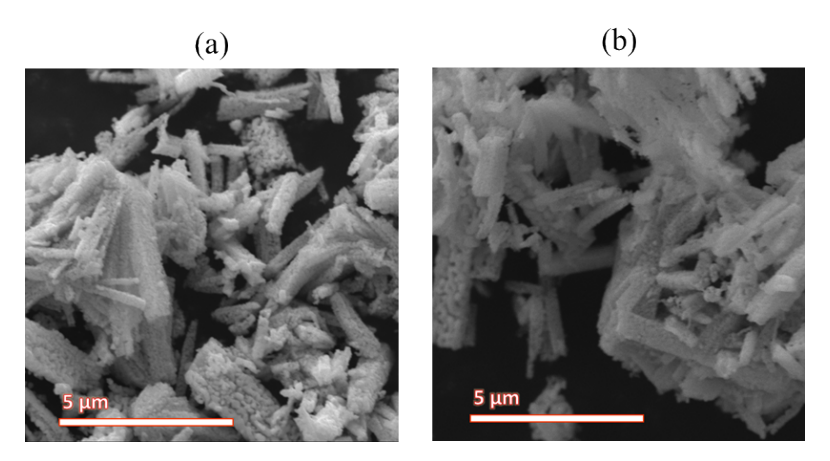


Figure 3. Scanning electron microscopy images Co₃Mo₃N particles (a) before and (b) after cycling experiments.

The EDS results in Figure 4 showed uniform distribution of (a) Co, (b) Mo, (c) O and (d) N, indicative of no phase segregation and consistent with previous XRD and elemental analysis. The strong oxygen signal suggested presence of oxide phases, which were not detected with XRD. The

oxide phase(s) were, therefore, expected in low concentrations and located mainly on the particle surface based the surface sensitivity of EDS.

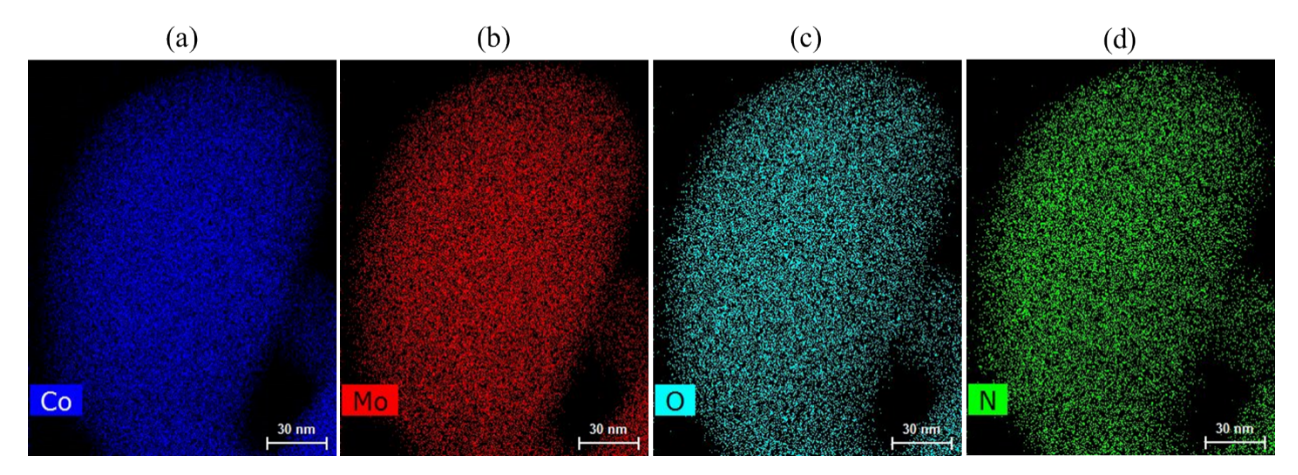


Figure 4. Atomic distribution of (a) Co, (b) Mo, (c) O and (d) N from energy dispersive X-ray spectroscopy.

Characterization of surface oxygen-rich layer: XPS and TEM analyses were used to further confirm and characterize the presence of oxygen-rich phases on particle surfaces that were below the XRD detection limits. TEM was performed for samples before and 1 h after removal from cycling in a thermogravimetric analyzer (TGA, Netzsch STA 449 F3 Jupiter, ± 1μg) to characterize the penetration of the surface oxygen on CMN331 samples, and the effects of sample exposure to O₂ in air. TEM images for a CMN331 sample are shown in Figure 5 for particle surface sites (a) before and (b) 1 h after cycling experiments in TGA under 5-10% H₂/Ar and 5-10% H₂/N₂. An amorphous layer ~2 nm thick was observed on the sample prior to cycling, and the thickness was significantly reduced to several atomic layers 1 h after cycling. Comparison with XPS and EDS results suggested that the amorphous phase was oxygen-rich. The clear boundary between the inner particle crystalline structure and the oxygen-rich surface amorphous layer indicated no penetration of the oxygen-rich phases into the bulk particle.

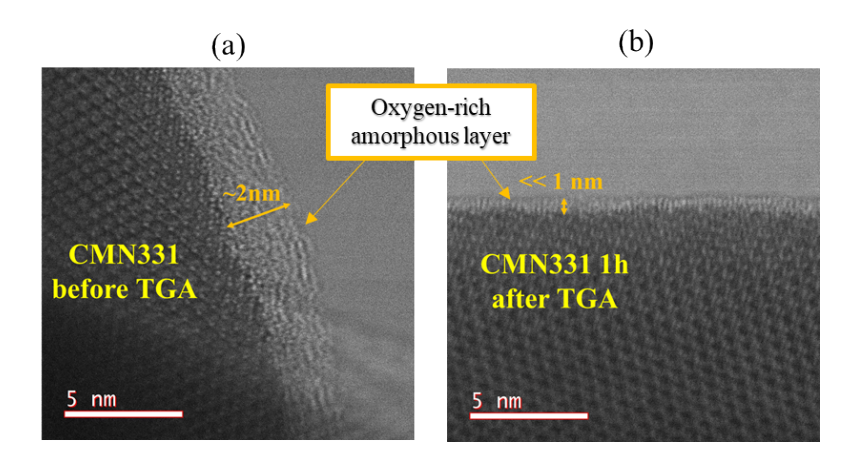


Figure 5. Particle surface oxygen-rich amorphous layer captured with transmission electron microscopy for a Co₃Mo₃N sample (a) before and (b) 1 h after cycling experiments.

XPS was performed with etching using an ion gun between each scan to investigate the distribution of oxygen-rich phases within samples. XPS results are shown in Figure 6 for (a) measured surface oxygen for two CMN331 samples before (solid black line and green dashed line), 30 min after (blue dotted line), and four days after (red dash-dotted line) cycling in TGA, y_0 represents atomic fraction of measured oxygen and N represents etch levels. XPS spectra are shown in Figure 6 for (b) before depth profiling and (c) after 26 depth profiling passes. The scans were performed on samples that were cycled under 5-10% H₂/Ar and 5-10% H₂/N₂. XPS measurements showed surface oxygen decreased significantly with increased etching, indicating that oxygen was more prevalent closer to particle surfaces rather than being evenly distributed through the bulk of the CMN. Significantly less surface oxygen was detected 30 min after cycling, but the oxygen level nearly returned to the initial value after four days of exposure to air. The results were highly repeatable between two different CMN331 samples prior to cycling.

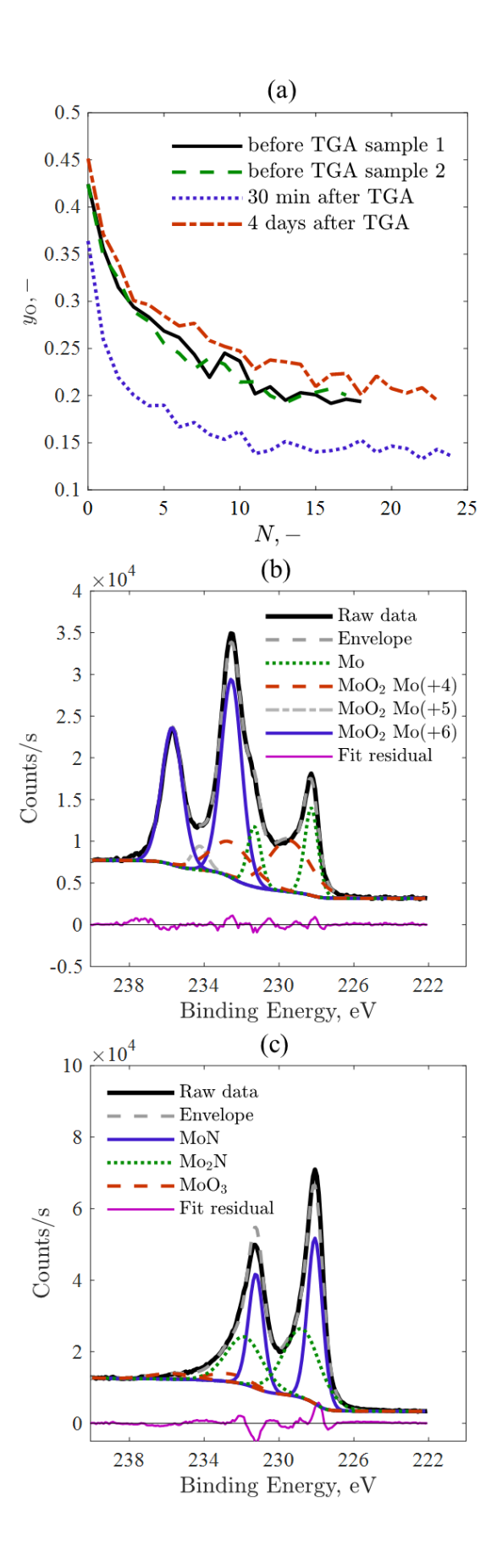


Figure 6. X-ray photoelectron spectroscopy analysis for (a) surface oxygen concentration of Co₃Mo₃N samples over each depth-profiling steps, where layers of materials were etched away using an ion gun between scans; scans were performed for samples before (solid black line and green dashed line), 30 min after (blue dotted line), and four days after cycling experiments (red dash-dotted line). Modeled X-ray photoelectron spectroscopy spectra are overlaid with the measurements in the Mo 3d region of a Co₃Mo₃N powder sample (b) before depth profiling, (c) after 26 depth profiling passes, where y_O represents atomic fraction of measured oxygen and N represents etch levels.

Oxides phases were determined to be the primary surface compositions as seen in the XPS spectra of the powder sample before depth-profiling (Fig. 6b). Elemental Mo at the solid surface before cycling under H_2 was likely a result of surface oxidation with a Mo and MoO₂ mixture present. Depth profiling resulted in the XPS spectra transitioning from metal oxides to nitrides (Fig. 6c) deeper in the bulk material. No detectable elemental Mo and MoO₂ suggest that these unwanted secondary phase(s) were not penetrating within the bulk material. An insignificant presence of MoO₃ phase was detected as seen in the XPS spectra after depth profiling. Metal nitride phases were confirmed by comparing with other known existing XPS spectra of common binary nitrides [e.g., MoN or Mo_2N (Supplementary Table S1)]. Effects of reactant gas treatment on CMN331 were examined in previous work [16]. Similar findings were produced with gas pretreatment of 75% H_2/N_2 at temperatures > 600 °C, increasing NH_3 production from CMN331 samples. A study on MoN_x thin films also observed the formation of surface oxide layers [31] that were removed during XPS surface depth-profiling. The formation of an oxygen-rich phase was also identified in previous work for CMN331 after passivation in 1% O_2/He , along with decrease in BET surface area [13].

XPS and TEM analyses indicated that exposure to O₂ in ambient air resulted in the formation of oxygen-rich phases on the CMN331 surface. The oxygen distribution from XPS analysis confirmed the critical role of H₂ in removing oxygen from CMN331 particle surfaces. Separation of secondary oxygen-rich phases from the bulk lattice structure of CMN331/661 at the surface, as observed by TEM, enabled oxygen removal via reactions with H₂ to form H₂O(v) during cycling at elevated temperatures.

2.2 Cycling under 75% H_2/Ar and 75% H_2/N_2

Cycling experiments with TGA under 5% H₂/Ar and 5% H₂/N₂ were initially performed for a powdered CMN331 sample at 1 bar (Supplementary Fig. S11), resulting in minimal NH₃ during

sample reduction step as discussed in Supplementary Information. Insufficient evidence of sample reduction suggested H₂ concentrations > 5% are needed to reduce CMN331 samples.

Reduction/nitridation cycling was performed for a CMN331 powder with 111.5 mg of sample in the tube furnace under 75% H₂/Ar and 75% H₂/N₂ with total pressure of 1 bar. Gas dispersion was characterized using a method similar to that described in [32]. No significant dispersion effects were observed on downstream measurements. NH₃ adsorption on surfaces was examined before experimentation by flowing 100 mL_N/min of 76.93 ppm NH₃/Ar gas through the tube furnace at 500 °C for 2.5 h before switching to 100% Ar. NH₃ was measured using MS and liquid conductivity meter. No noticeable NH₃ adsorption/desorption was observed under the investigated conditions for cycling experiments.

Cycling results in the tube furnace are shown in Figure 7 for reduction at 500 °C under 75% H₂/Ar and nitridation at 700 °C under 75% H₂/N₂ for (a) ion signals of H₂O(v) (18 amu, solid black line), NH₃ (17 amu, blue dotted line) and N₂ (28 amu, purple dashed line) measured using MS and (b) the liquid conductivity measurement of NH₃ for the experiment with (solid black line) and without a sample (green dashed line), and at reduction of 700 °C under 75% H₂/Ar and nitridation at 700 °C under 75% H₂/N₂ for (c) ionic signals and (d) measured NH₃ concentration. Cycling results are plotted against the measured furnace temperature (red dash-dotted line) and gas condition (75% H₂/Ar, yellow region and 75% H₂/N₂, purple region).

CMN331 was first subjected to two consecutive reduction/nitridation cycles with a reduction step at 500 °C under 75% H₂/Ar and a nitridation step at 700 °C under 75% H₂/N₂ after the overnight gas treatment step under 75% H₂/N₂ at 500 °C. Neither NH₃ nor N₂ was observed when the sample was heated under 75% H₂/Ar at 500 °C (yellow region) as measured by the MS and liquid conductivity measurement (Fig. 7a-b). The results indicated that the sample was not reduced, and NH₃ peaks previously observed at 500 °C under 5% H₂/Ar were likely due to surface adsorbed nitrogen reacting with H₂. NH₃ was observed during the nitridation under 75% H₂/N₂ due to thermodynamically favorable conditions. Comparison between cycling with and without

samples showed enhanced NH_3 production at 500 °C under 75% H_2/N_2 due to CMN catalytic activity where NH_3 yield is more favorable relative to 700 °C.

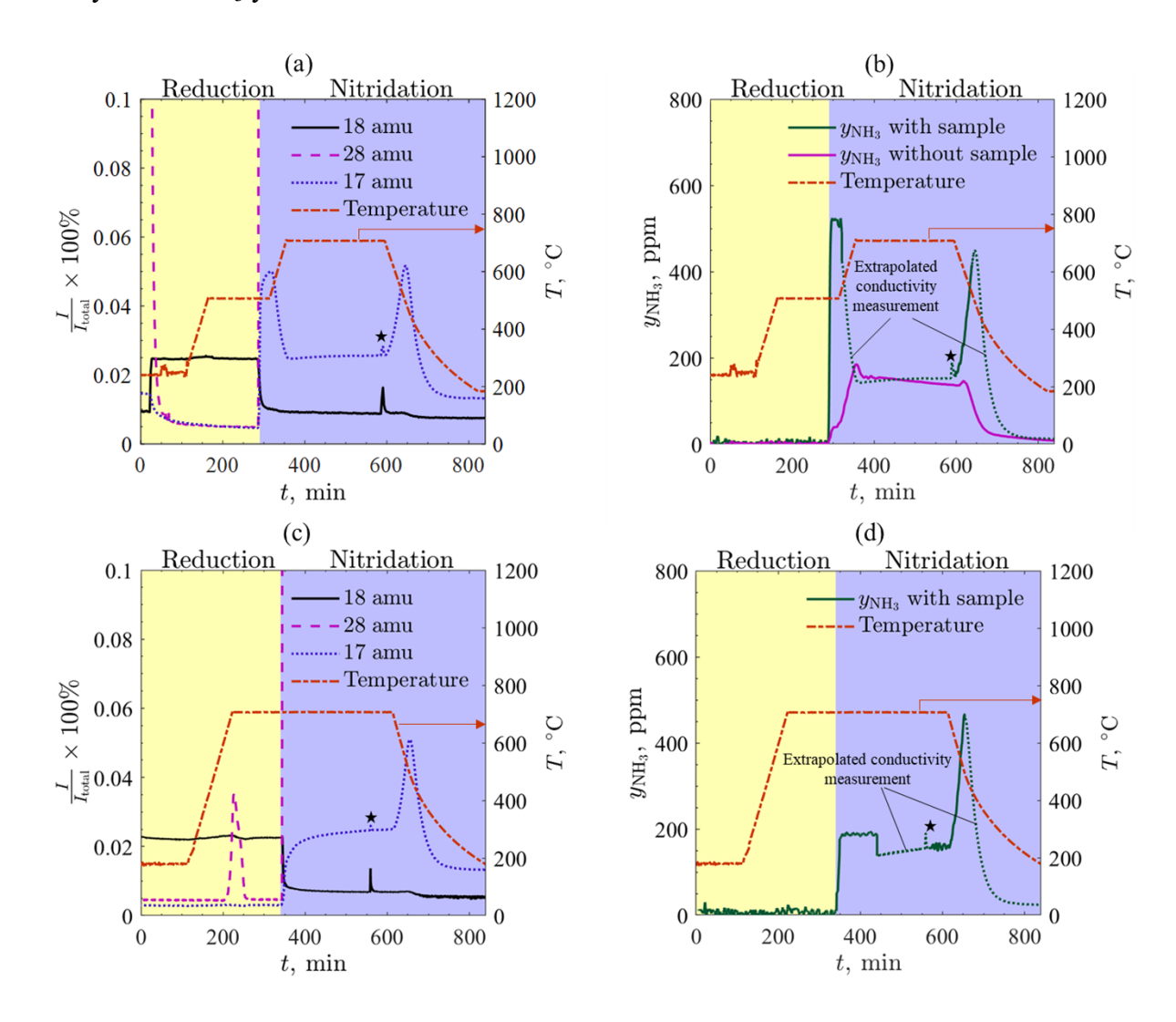


Figure 7. Co₃Mo₃N cycling results in tube furnace for a reduction step at 500 °C under 75% H₂/Ar (yellow region) and nitridation step at 700 °C under 75% H₂/N₂ (purple region) with (a) ionic signals of H₂O(v) (solid black line), NH₃ (blue dotted line), and N₂ (purple dashed line) measured using mass spectrometry and (b) measured NH₃ concentrations (with sample, solid black line and without sample, green dashed line); (c) and (d) show ion signals and measured NH₃ concentration for cycling with reduction step at 700 °C under 75% H₂/Ar (yellow region) and nitridation step at 700 °C under 75% H₂/N₂ (purple region). The red dash-dotted line represents the measured furnace temperature. The star indicates signal fluctuations due to pressure changes as conductivity meter solution was replaced. The black dotted line represents extrapolated conductivity measurement with MS calibrations.

Cycling with the same CMN331 powder sample without removal from the furnace followed with an isothermal reduction and nitridation step at 700 °C under 75% H₂/Ar and 75% H₂/N₂,

respectively. Sample reduction was observed under 75% H_2 /Ar at 700 °C, evidenced by evolving N_2 with no NH_3 detected (Fig. 7c-d). NH_3 production from CMN331 reduction under 75% H_2 /Ar at 700 °C was not thermodynamically favorable at the low pressures and elevated temperature used in this investigation.

The sample was then fully re-nitridized after heating to 700 °C for 4 h under 75% H_2/N_2 , where XRD of post-experiment sample also matched to a fully-nitridized CMN331 phase. Complete conversion to CMN331 was also observed when heating a CMN661 sample to 700 °C under 25% H_2/N_2 for 4 h (Supplementary Fig. S8b).

Results from the cycling suggest that temperatures > 500 °C are required to reduce CMN331 sample under 75% H₂/Ar, and elevated pressures are required to minimize NH₃ dissociation and increase yield according to Le Chatelier's principle. Minimizing NH₃ dissociation at elevated temperatures to overcome thermodynamic limitations was also achieved by altering surface mechanism(s) responsible for NH₃ production. Nitridation conditions of 700 °C under 25 to 75% H₂/N₂ were sufficient to fully regenerate CMN331 from CMN661. Reduction/nitridation of CMN331 and CMN661 are highly correlated to the components of the gas mixture, specifically the presence of Ar or N₂: 25-75% H₂/N₂ or 25-75% H₂/Ar. Favorable reduction/nitridation between CMN331 and CMN661 occurred isothermally by simply switching gases.

Presence of H_2 minimized formation of oxide phases as Co and Mo readily oxidize in presence of O_2 . H_2 is required to reduce CMN331 for NH_3 production and serves as a dual purpose to also remove O from particle surface. The identified oxygen-rich layer is removed before sample reduction to produce NH_3 , as evidenced by peak in $H_2O(v)$.

2.3 H₂ pressure-swings under 25 to 75% H₂/Ar

CMN331 reduction rates were examined using H₂ pressure-swing experiments under 25 to 75% H₂/Ar at temperatures of 700 °C and 650 °C and total pressure of 1 bar. Results from H₂ pressure-swings under 100% Ar (yellow region) to 75% H₂/Ar (purple region) are given in Figure 9 at (a) 700 °C and (b) 650 °C with N₂ (28 amu) from MS (solid black line) and NH₃ concentration from liquid conductivity measurement with sample (solid green line) and without sample (solid purple line), plotted against measured furnace temperature (red dash-dotted line). MS signals were baselined by a blank experiment to offset fluctuations in line pressure from the gas switch. Larger

fluctuations that were not completely offset upon the gas switch point resulted in artefacts (spikes) in MS results. Small N₂ peaks were observed when the samples were heated to > 600 °C in 100% Ar, indicative of N₂ desorption. The onset of sample reduction was immediately observed after gas switches from 100% Ar to 75% H₂/Ar at both temperatures, evidenced by significant increases in N₂ and NH₃. Isothermal H₂ pressure-swings resulted in measurable NH₃ in 75% H₂/Ar, compared to no detectable NH₃ when samples were gradually heated from temperatures < 200 °C to 700 °C under 75% H₂/Ar (Fig. 7d). An earlier onset of N₂ desorption at 600 °C compared to sample reduction at > 650 °C suggests adsorbed surface nitrogen affected NH₃ production. A small NH₃ peak was detected upon H₂ pressure-swing from 100% Ar to 75% H₂/Ar during baseline experiments without a sample, suggesting a small fraction of NH₃ observed originated from H₂ reacting with residual nitrogen adsorbed by inner reactor tube walls. Elevated H₂ pressures were observed to increase the total produced NH₃ during H₂ pressure-swing reduction.

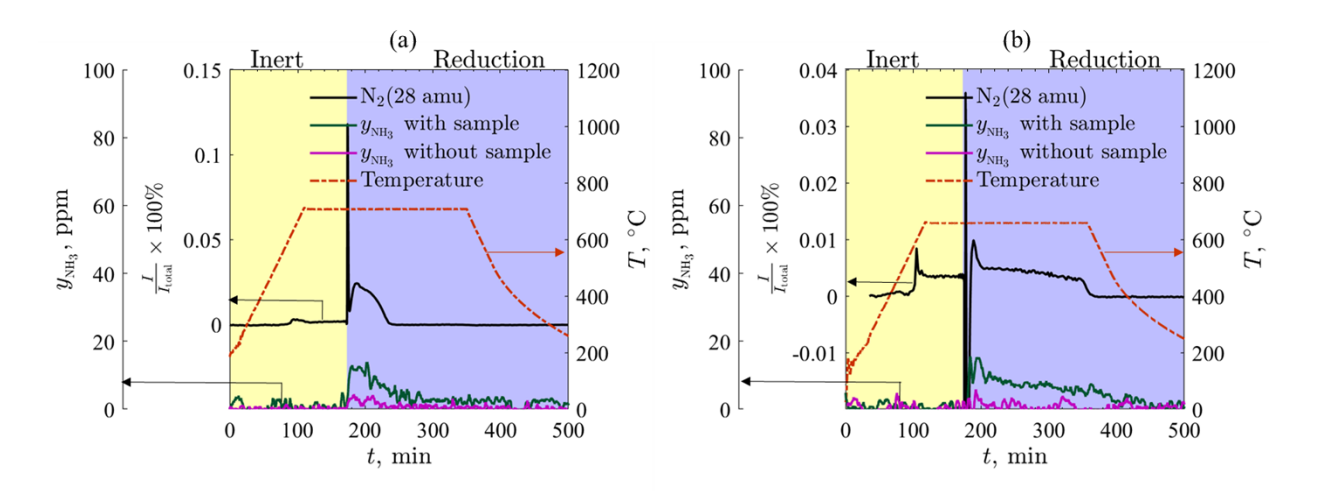


Figure 9. Co₃Mo₃N H₂ pressure-swing measurements under 100% Ar (yellow region) and 75% H₂/Ar (purple region) at (a) 700 °C and (b) 650 °C, showing normalized N₂ concentration (solid black line) measured by mass spectrometry, NH₃ concentration with sample (solid green line) and baseline NH₃ concentration without sample (solid purple line) determined by liquid conductivity measurement, plotted against measured furnace temperature (red dash-dotted line).

The molar ratios of NH₃ produced to the initial CMN331 were $n_{\text{NH3}}/n_{\text{CMN331}} = 0.0307$ and 0.0161 for H₂ pressure-swings to 75% H₂/Ar at 650 and 700 °C, respectively. Increased relative NH₃ for H₂ pressure-swings at 650 °C was likely due to NH₃ formation being more thermodynamically favorable at lower temperatures. The N₂ and NH₃ evolution profiles indicated a total reduction time of ~70 min at 700 °C under 75% H₂/Ar, and the reduction at 650 °C was still incomplete after 3 h under the same partial H₂ pressures. H₂ pressure-swings between 100% Ar

and 25% H₂/Ar at 700 °C (Supplementary Fig. S3) showed complete sample reduction within ~140 min, indicating that the reduction reaction rates were strongly correlated to H₂ partial pressure and temperature. XRD analyses matched the samples reduced at 700 °C under 75% H₂/Ar to a single CMN661 phase, indicative of full sample reduction, while a mixture of CMN331 and CMN661 phases was observed in the sample that underwent H₂ pressure-swings at 650 °C under 75% H₂/Ar (Fig. 2b), evidence that full reduction was not achieved. H₂ pressure-swing reduction at 700 °C under 25% H₂/Ar also led to complete conversion of CMN331 sample to CMN661 after 3 h under as shown in Supplementary Figure S4.

H₂ pressure-swings for CMN331 led to more NH₃, where higher temperature of 700 °C was needed to fully reduce CMN331 within 70 min under 75% H₂/Ar and 140 min under 25% H₂/Ar. Five consecutive cycles were performed with a CMN sample undergoing H₂ pressure-swing reduction to produce NH₃ at 700 °C under 75% H₂/Ar, and nitridation at 700 °C under 75% H₂/N₂. Consistent NH₃ production (Supplementary Table S4) during H₂ pressure-swing reduction was observed between cycles. XRD analysis showed no change in sample crystallographic structure from cycling (Supplementary Figure S10). H₂ pressure-swing results demonstrate successful NH₃ production from CMN331 reduction at 1 bar and suggest higher total pressures are needed to minimize NH₃ dissociation and improve production of NH₃ relative to N₂ in a CST NH₃ reactor. One benefit of the proposed NH₃ production process is the lower operating pressures compared to Haber-Bosch. The required elevated temperatures correlate with lower NH₃ at chemical equilibrium which is addressable by altering the reaction mechanism of NH₃ formation. NH₃ is very refractory and the decomposition is kinetically hindered at these temperatures so that chemical equilibrium compositions are not reached. Results from H₂ pressure-swing reduction indicated the feasibility of increasing NH₃ yields at the same temperature and H₂ partial pressure by adjusting the initial heating step.

3. Conclusions

A two-step solar thermochemical looping cycle was examined based on Co₃Mo₃N/Co₆Mo₆N reduction/nitridation for producing NH₃ from H₂ and N₂. The reduction/nitridation capacities were investigated by cycling and H₂ pressure-swing reduction experiments. NH₃ was detected and quantified during CMN331 reduction using MS and liquid conductivity measurement. Material characterization was performed with a combination of XRD, SEM/EDS, elemental analysis, XPS,

and TEM. The presence of an oxygen-rich surface layer on the samples several atomic layers to \sim 2 nm in thickness was observed with EDS, XPS, and TEM due to exposure to air and trace O_2 , which was minimized by adding H_2 to the reducing flows.

Co₃Mo₃N reduction to NH₃ was investigated under 25 to 75% H₂/Ar at temperatures between 500 and 700 °C under atmospheric pressure to form Co₆Mo₆N. Evidence of Co₃Mo₃N reduction was observed at H₂ concentrations ≥ 25% H₂/Ar, accompanied by significant NH₃ production when H₂ pressure-swings were adopted. Temperatures > 500 °C were necessary to reduce Co₃Mo₃N and increased H₂ pressures at 700°C pressures led to more rapid reductions and enhanced NH₃ production. H₂ pressure-swing reduction increased NH₃, an important result that will inform future development of NH₃ synthesis reactors driven by concentrated solar thermal technologies. Complete regeneration of Co₃Mo₃N from Co₆Mo₆N was observed when heating samples to 700 °C under 25 to 75% H₂/N₂ for 4 h. Cycling at elevated pressures was proposed for improving overall NH₃ yield, based on thermodynamic forecasting.

The work represents the first comprehensive characterization of non-catalytic NH_3 production in a two-step solar thermochemical looping cycle based on nitride reactions. The cycle, when coupled with N_2 sourced from solar thermochemical air separation and H_2 from solar thermochemical H_2O splitting, represents a fully renewable path towards large-scale NH_3 production.

4. Experimental Procedures

A series of experiments was conducted to characterize and examine reduction extents of Co₃Mo₃N for chemical looping to produce NH₃. Gas mixtures of 100% Ar to 75% H₂/Ar and 100% N₂ to 75% H₂/N₂ from H₂ produced by an H₂-generator (100ccm, Airgas) mixed with pure Ar and N₂ (UHP, Airgas) using flow controllers (Bronkhorst EL-FLOW Select).

4.1 Synthesis methodology

CMN331 samples were synthesized by nitridizing CoMoO₄ powder samples in 10% H₂/N₂ at 805 °C in a tube furnace (MTI GSL-1700X) following a gradual stepping temperature schedule [19, 33]. Samples were mounted in a 1" OD tube with an Al₂O₃ boat containing samples with masses between 100 and 200 mg with 100 mL_N/min of flowing gas (where L_N refers to liters at

standard conditions: 273 K and 1 bar). CoMoO₄ powder samples were spread \leq 1 mm thick on an Al₂O₃ boat to maximize mass transfer during synthesis.

4.2 Material characterization

Powder XRD (PANalytical X'Pert PRO Alpha-1 diffractometer with Cu Kα radiation) and whole pattern matching (HighScore, PDF-4+ 2022) were used to verify crystalline structures before and after reduction/nitridation experiments and confirm that all starting samples were single-phase before experimentation. Elemental analysis was performed using ICP-OES (Perkin-Elmer Optima 5300 DV) and combustion analysis (Perkin-Elmer 2400 Series II CHNS/O Analyzer) to confirm sample stoichiometry. Samples before and after cycling were examined via SEM and EDS (Phenom ProX G5 SEM) at scanning voltage of 15 kV. XPS (Thermo K-Alpha, Al K-Alpha source) was used to further examine the particle surface elemental distributions. TEM (Hitachi HD2700) was used to visually inform presence of secondary phases outside of the CMN331 lattice.

4.3 Reduction/nitridation cycling

Reduction/nitridation cycling for CMN331 was performed in a tube furnace (MTI GSL-1700X) with 75% H₂/Ar and 25-75% H₂/N₂ to investigate sample nitrogen capacities and favorable conditions for producing NH₃. The experiment schematic is shown in Supplementary Figure S1. MS (OmniStar GSD 320) was used to measure product gas concentrations at the TGA and furnace outlets with ion signals of 28 amu (N₂) and 17 amu (NH₃) to directly probe sample reduction. NH₃ fragments (15, 16 and 17 amu) were detected during both the reduction and the nitridation using the MS, where 15 amu is unique to NH₃, [*i.e.*, other species (O₂, H₂O) in the gas stream do not produce this peak] (Supplementary Table S2).

NH₃ in the exhaust gas was also measured using a liquid conductivity meter (Orion Star A212, Thermo Fisher Scientific) to compensate for the sensitivity of the MS to small pressure fluctuations in the flow. The exhaust gases were bubbled through a beaker containing 500 mL of 0.00012 M H₂SO₄ in deionized H₂O(1), where free H⁺ reacted with NH₃ to form (NH₄)₂SO₄ [34]. The beaker was placed in an insulative foam container filled with H₂O(1) to minimize temperature fluctuations and mitigate uncertainties. A K-type thermocouple was submerged in the solution to account for the solution change in conductivity due to temperature fluctuations. NH₃ rates under 25 to 75%

H₂/N₂ at 500 and 700 °C were examined from liquid conductivity measurements by averaging results at equilibrium region after gas switch. Calibrations were performed to correlate the resulting changes in the solution ionic conductivity to both temperature changes and to NH₃ concentration in the gas stream. Low molarities of the H₂SO₄ solution facilitated higher resolutions for conductivity measurements, but they also resulted in conductivity saturation outside of the calibration range during nitridation with significant levels of NH₃. The MS signals were, therefore, correlated to in-range conductivity measurements and extrapolated to predict the NH₃ concentrations.

Additional experimental protocols were adopted to minimize NH_3 adsorption on the inner tubing surfaces and to accurately measure *in-situ* NH_3 . Sulfinert coated stainless steel and PTFE with $\frac{1}{4}$ " outer diameter tubes were installed for the exhaust and bubbler lines, respectively, and both were maintained at ~170 °C to minimize NH_3 adsorption onto the inner surfaces.

Undesired sample oxidation was mitigated by adopting prevention steps to minimize residual O_2 in the reaction chamber (e.g., minimizing leakage in gas lines and using O_2 scrubbers).

Reduction/nitridation cycling under 75% H_2/Ar and 25-75% H_2/N_2 was performed using a horizontal tube furnace to examine the impacts of higher H_2 concentrations. A CMN331 sample with a mass of 111.5 mg was spread < 1 mm in thickness on an Al_2O_3 boat to minimize bulk diffusion limitations. The sample was heated to 500 °C under 75% H_2/N_2 overnight prior to experimentation to minimize sample surface oxygen from the oxygen-rich layer and adsorption, and to off-gas moisture. The sample temperatures were maintained between 180 and 200 °C between cycles to limit adsorption of trace O_2 and $H_2O(v)$ in the gas stream. Two cycling schedules were used to investigate reduction/nitridation of the CMN331 powder sample: (1) reduction at 500 °C followed by nitridation at 700 °C and (2) isothermal reduction followed by nitridation at 700 °C. Samples were reduced under 75% H_2/Ar for 2 h and nitridized at 700 °C for 4 h under 25-75% H_2/N_2 . Cycling without samples was performed in the tube furnace following similar schedules to baseline the NH₃ measurements under 25-75% H_2/N_2 , allowing for examination of CMN331 catalytic effects up to 700 °C [13, 35].

4.4 H₂ pressure-swing reduction

CMN331 reduction reaction rates were examined under 25-75% H₂/Ar and temperatures of 650 and 700 °C in the tube furnace. CMN331 samples (140 -160 mg) were spread into a layer < 1mm in thickness on an Al₂O₃ boat. The H₂ pressure-swings began with the temperature ramp to 650 or 700 °C under 100% Ar at 5 K/min, and samples were held isothermally for 1 h. A gas switch from 25 to 75% H₂/Ar followed to promote sample reduction, where the sample was held isothermally for 3 h, then cooled to ambient temperature. MS and liquid conductivity meter measurements were used to monitor gas compositions and quantify NH₃. Blank experiments with no samples were performed to correct for MS signal fluctuations during gas switches due to disruptions in the exhaust line pressure.

Acknowledgements

This material is based upon work supported by the U.S. Department of Energy's Office of Energy Efficiency and Renewable Energy (EERE) under the Solar Energy Technologies Office (SETO) Award Number DE-EE0034250. This article has been authored by an employee of National Technology & Engineering Solutions of Sandia, LLC under Contract No. DE-NA0003525 with the U.S. Department of Energy (DOE). The employee owns all right, title and interest in and to the article and is solely responsible for its contents. The United States Government retains and the publisher, by accepting the article for publication, acknowledges that the United States Government retains a non-exclusive, paid-up, irrevocable, world-wide license to publish or reproduce the published form of this article or allow others to do so, for United States Government purposes. The DOE will provide public access to these results of federally sponsored research in accordance with the DOE Public Access Plan https://www.energy.gov/downloads/doe-public-access-plan.

Declaration of Interests

All authors declare no competing interests.

References

- 1. Kobayashi, H., et al., *Science and technology of ammonia combustion*. Proceedings of the Combustion Institute, 2019. **37**(1): p. 109-133.
- 2. IEA, *Ammonia Technology Roadmap*. IEA, 2021. **Paris**(https://www.iea.org/reports/ammonia-technology-roadmap).

- 3. Liu, H., Ammonia synthesis catalysts: innovation and practice. 2013: World Scientific.
- 4. Boyano, A., et al., Exergoenvironmental analysis of a steam methane reforming process for hydrogen production. Energy, 2011. **36**(4): p. 2202-2214.
- 5. Wang, B. and L. Shen, *Recent advances in NH*₃ synthesis with chemical looping technology. Industrial & Engineering Chemistry Research, 2022. **61**(50): p. 18215-18231.
- 6. Fu, E., et al., Chemical looping technology in mild-condition ammonia production: A comprehensive review and analysis. Small, 2023. n/a(n/a): p. 2305095.
- 7. Brown, S. and J. Hu, *Review of chemical looping ammonia synthesis materials*. Chemical Engineering Science, 2023. **280**: p. 119063.
- 8. Gao, W., et al., *Production of ammonia via a chemical looping process based on metal imides as nitrogen carriers.* Nature Energy, 2018. **3**(12): p. 1067-1075.
- 9. Doornkamp, C. and V. Ponec, *The universal character of the Mars and Van Krevelen mechanism*. Journal of Molecular Catalysis A: Chemical, 2000. **162**(1): p. 19-32.
- 10. McKay, D., et al., *Towards nitrogen transfer catalysis: reactive lattice nitrogen in cobalt molybdenum nitride.* Chemical Communications, 2007(29): p. 3051-3053.
- 11. Tricker, A.W., et al., *Mechanocatalytic ammonia synthesis over TiN in transient microenvironments*. ACS Energy Letters, 2020. **5**(11): p. 3362-3367.
- 12. Ye, T.-N., et al., Contribution of nitrogen vacancies to ammonia synthesis over metal nitride catalysts. Journal of the American Chemical Society, 2020. **142**(33): p. 14374-14383.
- 13. Kojima, R. and K.-i. Aika, Cobalt molybdenum bimetallic nitride catalysts for ammonia synthesis: part 1. preparation and characterization. Applied Catalysis A: General, 2001. **215**(1): p. 149-160.
- 14. Boisen, A., S. Dahl, and C.J.H. Jacobsen, *Promotion of binary nitride catalysts: isothermal* N_2 adsorption, microkinetic model, and catalytic ammonia synthesis activity. Journal of Catalysis, 2002. **208**(1): p. 180-186.
- 15. Jacobsen, C.J.H., et al., Catalyst design by interpolation in the periodic table: bimetallic ammonia synthesis catalysts. Journal of the American Chemical Society, 2001. **123**(34): p. 8404-8405.
- 16. Kojima, R. and K.-i. Aika, *Cobalt molybdenum bimetallic nitride catalysts for ammonia synthesis: part 3. Reactant gas treatment.* Applied Catalysis A: General, 2001. **219**(1): p. 157-170.
- 17. Hunter, S.M., et al., *A study of* ¹⁵*N*/¹⁴*N isotopic exchange over cobalt molybdenum nitrides*. ACS Catalysis, 2013. **3**(8): p. 1719-1725.
- 18. Gregory, D.H., J.S.J. Hargreaves, and S.M. Hunter, *On the regeneration of Co*₃*Mo*₃*N from Co*₆*Mo*₆*N with N*₂. Catalysis Letters, 2011. **141**(1): p. 22-26.
- 19. Hunter, S.M., et al., *Topotactic nitrogen transfer: structural transformation in cobalt molybdenum nitrides.* Chemistry of Materials, 2010. **22**(9): p. 2898-2907.
- 20. Hargreaves, J.S.J., *Nitrides as ammonia synthesis catalysts and as potential nitrogen transfer reagents.* Applied Petrochemical Research, 2014. **4**(1): p. 3-10.
- Farr, T.P., et al., An A- and B-site substitutional study of $SrFeO_{3-\delta}$ perovskites for solar thermochemical air separation. Materials, 2020. **13**(22).
- 22. Nguyen, N.P., et al., Air separation via two-step solar thermochemical cycles based on $SrFeO_{3-\delta}$ and $(Ba,La)_{0.15}Sr_{0.85}FeO_{3-\delta}$ perovskite reduction/oxidation reactions to produce N_2 : rate limiting mechanism(s) determination. Physical Chemistry Chemical Physics, 2021. **23**(35): p. 19280-19288.

- 23. Bush, H.E., R. Datta, and P.G. Loutzenhiser, *Aluminum-doped strontium ferrites for a two-step solar thermochemical air separation cycle: Thermodynamic characterization and cycle analysis.* Solar Energy, 2019. **188**: p. 775-786.
- Bush, H.E., et al., Air separation via a two-step solar thermochemical cycle based on $(Ba,La)_xSr_{1-x}FeO_{3-\delta}$: thermodynamic analysis. Solid State Ionics, 2021. **368**: p. 115692.
- 25. Schieber, G.L., et al., H_2O splitting via a two-step solar thermoelectrolytic cycle based on non-stoichiometric ceria redox reactions: thermodynamic analysis. International Journal of Hydrogen Energy, 2017. **42**(30): p. 18785-18793.
- 26. Charvin, P., et al., Two-step water splitting thermochemical cycle based on iron oxide redox pair for solar hydrogen production. Energy, 2007. **32**: p. 1124-1133.
- 27. Boretti, A., Concentrated solar energy with thermal energy storage for hydrogen production by three-step thermochemical water-splitting cycles. Energy & Fuels, 2021. **35**(13): p. 10832-10840.
- 28. Romero, M. and A. Steinfeld, *Concentrating solar thermal power and thermochemical fuels*. Energy & Environmental Science, 2012. **5**(11): p. 9234-9245.
- 29. Steinfeld, A. and A.W. Weimer, *Thermochemical production of fuels with concentrated solar energy*. Optics Express, 2010. **18**(S1): p. A100-A111.
- 30. de la Calle, A., et al. *Techno-economic analysis of solar-thermal ammonia production*. in *SolarPACES*. 2022. United States.
- 31. Fix, R., R.G. Gordon, and D.M. Hoffman, Low-temperature atmospheric-pressure metalorganic chemical vapor deposition of molybdenum nitride thin films. Thin Solid Films, 1996. **288**(1): p. 116-119.
- 32. Evan Bush, H., et al., Design and characterization of a novel upward flow reactor for the study of high-temperature thermal reduction for solar-driven processes. Journal of Solar Energy Engineering, 2017. **139**(5).
- 33. Gao, X., et al., *Synthesis and structural study of substituted ternary nitrides for ammonia production.* Chemistry of Materials, 2023.
- 34. Shaw, J. and B.W. Staddon, *A conductimetric method for the estimation of small quantities of ammonia.* Journal of Experimental Biology, 1958. **35**(1): p. 85-95.
- 35. Aslan, M.Y., J.S.J. Hargreaves, and D. Uner, The effect of $H_2: N_2$ ratio on the NH_3 synthesis rate and on process economics over the Co_3Mo_3N catalyst. Faraday Discussions, 2021. **229**(0): p. 475-488.